**Moroccan Journal of Chemistry**
**ISSN : 2351-812X**


**Mor. J. Chem., 2023, Volume 11, Issue 02, Page 411-433**
https://revues.imist.ma/index.php/morjchem

# Comparative study of inhibitory efficacy of methionine and its derivatives in acidic medium by mild steel

**Zaidi K.[1*], Aouniti A.[1**], Merimi C.[1], Daoudi W.[2], Dagdag O.[3], Berisha A.[4], Oussaid A.[2], Touzani R.[1], Messali M.[5], Hammouti B.[1,6]**

[1]*Laboratory of Applied Chemistry and Environment (LCAE), Faculty of Sciences, University Mohammed Premier, 60000 Oujda, Morocco*

[2]*Laboratory of Molecular Chemistry, Materials and Environment (LCM2E), Department of chemistry, Multidisciplinary Faculty of Nador, University Mohamed I, 60700 Nador, Morocco*

[3]*Centre for Materials Science, College of Science, Engineering and Technology, University of South Africa, Johannesburg 1710, South Africa*

[4]*Department of Chemistry, Faculty of Natural and Mathematics Science, University of Prishtina, 10000 Prishtina, Kosovo*

[5]*Department of Chemistry, College of Science, Imam Mohammad Ibn Saud Islamic University, P.O. Box, 90950, Riyadh 11623, Saudi Arabia*

[6]*Laboratory of Industrial Engineering, Energy and the Environment (LI3E), SupMTI, Rabat, Morocco.*

**Corresponding author, Email address: zaidikaoutar96@gmail.com*
**Corresponding author, Email address: aouniti@yahoo.fr*

***Received*** *05 Jan 2023,*
***Revised*** *21 Feb 2023,*
***Accepted*** *24 Feb 2023*

***Citation****: Zaidi K., Merimi C., Daoudi W., Dagdag O., Berisha A., Aouniti A., Oussaid A., Touzani R., Messali M., Hammouti B., Comparative study of inhibitory efficacy of methionine and its derivatives in acidic medium by mild steel Mor. J. Chem., 14(2), 411-433. Doi: https://doi.org/10.48317/IMIST.PRSM/morjchem-v11i2.38246*

**Abstract:** Corrosion inhibition effect of L-Methionine ($MT_1$), L-Methionine sulfoxide ($MT_2$) and L-Methionine sulfone ($MT_3$) on mild steel corrosion in 1M HCl solution was studied by using weight loss, electrochemical polarization and electrochemical impedance spectroscopy (EIS) techniques. The experimental results showed that the inhibitory efficiency of the three aminoacids improves with the increase of concentration to reach the maximum value of 95.20% for $MT_1$, 94.14% for $MT_2$ and 88.92% for $MT_3$ for a concentration of $10^{-3}$M, which translates that the surface covered by the inhibitor increases with the concentration. The effect of temperature on the corrosion rate was investigated and some thermodynamic parameters were calculated. Polarization studies show that three studied inhibitors suggested that three inhibitors control the anodic as well as cathodic reactions and act as mixed type in nature. The results show that $MT_1$, $MT_2$ and $MT_3$ are good inhibitors, and the adsorption of each inhibitor on mild steel surface obeys Flory-Huggins and Langmuir, with a better fit of the Langmuir isotherm through mixed adsorption (physisorption as well as chemisorption) process. In addition, the quantum approach based on density functional theory (DFT), monte Carlo (MC) and molecular dynamics (MD) simulations was confirmed the reactivity of the studied compound towards the corrosion process.

**Keywords:** mild steel; HCl: corrosion inhibition; aminoacids; Methionine; DFT

## 1. Introduction

Mild steel (MS) is a low cost highly demanded alloy in industries because it has a lot of good properties such as inherent flexibility, ductility, malleability, hardness, tensile strength, and high melting point (Paul and Yadav,2020) For this reason, researchers have long been interested in studying

the corrosion of mild steel in various corrosive environments (Abdallah *et al*.,2021, Dkhireche *et al*.,2020, El Aatiaoui *et al*., 2022, Mehta *et al*., 2022). It's known that the efficiency of an organic compound as corrosion inhibitor depends not only on the characteristics of the environment in which it acts, the nature of the metal surface and electrochemical potential at the interface, but also on the structure of the inhibitor itself. The inhibitor molecule should have centres capable of forming bonds with the metal surface via electron transfer. Thus, the metal acts as an electrophile, whereas the inhibitor molecule acts as a Lewis base, whose nucleophilic centre are normally available for sharing, i.e. formation of a bond. The application of organic compounds containing nitrogen, oxygen and sulfur as corrosion inhibitor in acid medium is reported in literature (Umoren *et al*.,2015, Nahl´e *et al*., 2021, Kaczerewska *et al*., 2017, Abd El-Lateef *et al*., 2020, Haldhar *et al*., 2021, Merimi *et al*.,2023, Merimi *et al*., 2023).

To date, a large number of inorganic and organic corrosion inhibitors have been studied, but most of them are toxic and hazardous to the environment, violating the current concept of green development. Hence, it is highly desirable to develop green, cost-effective and highly efficient corrosion inhibitors. The various researches showed that aminoacids exhibited as efficient corrosion inhibitors for steel, iron and copper in different test solutions (Kesavan *et al*.,2012, Sudheer *et al*., 2012, Jose Santana *et al*., 2012, Aytac *et al*., 2012, Chetouani *et al*., 2012; Loukili *et al*. 2022). However, some expensive self-assembled monolayers (SAMs) are organic compounds that are difficult to degrade and that might a toxic threat to environment. Therefore, eco-friendly SAMs are an urgent need. l-methionine [$CH_3$-S-$CH_2$-$CH_2$-CH($CO_2H$)$NH_2$], a molecule that contains both (-$NH_2$) and (-S-$CH_3$) groups, is biodegradable and relatively economical compared with traditional SAMs. This sulfur containing amino acid has been found to be an efficient molecule for self-assembled films and corrosion inhibitors (Zhang et al., 2015, Hammouti el al. 1995; Zerfaoui et al. 2002; Aouniti et al. 2022;).

In this study, we investigated the protection from corrosion of MS in acidic media by self- assembling l-methionine and its derivatives, as shown in **Figure 1**. Electrochemical techniques were used to study the inhibition efficiency of these self- assembled films on CS in a 0.5 M HCl solution.

The corrosion inhibition properties of three aminoacids: l-methionine, l-methionine sulfoxide and l-methionine sulfone inhibitor was analysed by weight loss and electrochemical studies as well using quantum chemical calculations to better understand the interaction mode of the inhibitors on the mild steel surface.

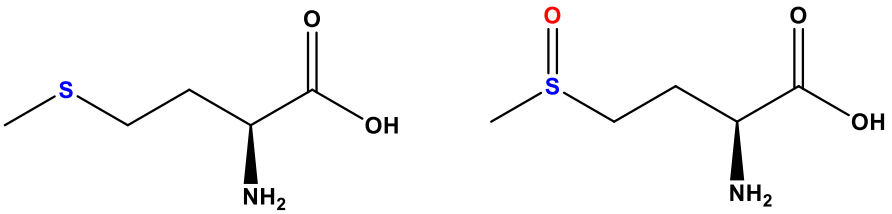


**L-methionine ($MT_1$)**




**L-methionine sulfoxide ($MT_2$)**

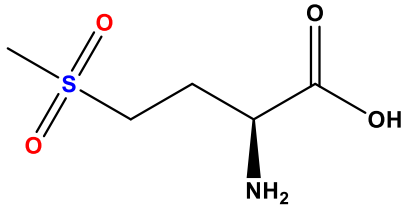


**L-methionine sulfone ($MT_3$)**

**Figure 1.** Chemical structure of methionine and its derivatives.

## 2. Materials and Experimental Methods

### *2.1. Material and study medium*

The samples used in this work are mild steel coupons with an average composition (% by weight) of 0.21C, 0.38Si, 0.05 Mn, 0.09P, 0.05S, 0.01Al and the rest iron, are used for electrochemical tests and mass loss. For the weight loss study, MS sheet was cut into pieces of dimension 1.5× 1.5 × 0.3 cm and for the electrochemical study mild steel electrode was prepared with 0.5cm$^2$ of exposed area to the acid solution. Before each experiment, the mild steel and pure iron electrodes were polished with 360, 400, 600, 800, 1200 grades of emery paper down to a mirror-like surface, degreased in pure acetone, and washed in distilled water and finally dried with tissue paper.

L-Methionine ($MT_1$) and L-Methionine sulfoxide ($MT_2$) and L-Methionine sulfone ($MT_3$) were purchased from Sigma- Aldrich and utilized as received without further purification.

The corrosive medium is prepared from the commercial solution of hydrochloric acid HCl, 37%, d = 1.19 and distilled water. The solution of 1M HCl was prepared by dilution of the commercial solution of hydrochloric acid HCl, 37%, d = 1.19. Stock solutions of $MT_1$ and $MT_2$ and $MT_3$ were prepared in 1M HCl and the required concentrations were dissolved in 1M HCl solution to obtain a concentration range of $10^{-6}$ to $10^{-3}$M.

### *2.2. Mass loss measurements*

Among the techniques used in this work to monitor corrosion, mass loss is simple, reliable and easy to conduct. The weight of sample before and after 6 h of submersion at 293–333K temperature in hydrochloric acid (1 M) and at various concentrations of inhibitors was recorded carefully by digital balance and loss in mass was calculated. In order to get good reproducibility, all measurements were performed few times and average values were reported to obtain good reproducibility. By using the weight loss data, the parameters of corrosion such as rate of corrosion (**CR**), surface coverage (**θ**) and inhibition efficiency (**$E_w$ (%)**) were evaluated by using equations Eqn.1, Eqn.2, Eqn.3 (Karthik and Sundaravadivelu, 2017)

$$CR = \frac{Weight\ loss}{Area\ (cm^2) \times time\ (h)} \qquad \textbf{Eqn.1}$$

$$\theta = \left(1 - \frac{CR}{CR_0}\right) \qquad \textbf{Eqn.2}$$

$$Ew\ (\%) = \left(1 - \frac{CR}{CR_0}\right) \times 100 \qquad \textbf{Eqn.3}$$

Where: $CR_0$ and CR are mild steel corrosion rates (mg cm$^{-2}$ h$^{-1}$) in the absence and presence of the extract, respectively.

### *2.3. Electrochemical techniques*

#### *2.3.1. Potentiodynamic polarization (PDP)*

The measurement of current density with and without the inhibitors, between the working electrode (mild steel) and the platinum electrode (auxiliary electrode) in the presence of a saturated calomel reference electrode (ECS), enable to estimate the inhibitory efficiency (ηEIS (%)) according to equation (4), using a PGZ100 potentiostat/ galvanostat monitored by a computer via Volta Master 4 software at the temperature 308 K. For all the electrochemical tests, the potential-current curves are recorded from cathodic to the anodic direction in a range between -200 mV and 800 mV/ESC, with a

scan rate of 0.5 mV/s in inhibited and uninhibited solution. The open circuit potential (OCP) was recorded as a function of time up to 30 min. As a result, Ecor which corresponds to a steady-state OCP was obtained before each test.

$$\eta EIS\,(\%) = \left(\frac{i_{cor}{}^{\circ} - i_{cor}}{i_{cor}{}^{\circ}}\right) \times 100 \qquad \textbf{Eqn.4}$$

Where $\mathbf{i_{cor}}^{\circ}$ and $\mathbf{i_{cor}}$ are, respectively, current densities before and after addition of the inhibitor.

### *2.3.2. Electrochemical impedance spectroscopy (EIS)*

The EIS experiments were conducted in the frequency range 100 KHz - 10 mHz using AC signals of amplitude 10 mV. EIS experiments were performed at OCP.The inhibition efficiency of the inhibitor was calculated from the charge transfer resistance values using the following equation in Eqn.5

$$\eta EIS\,(\%) = \left(\frac{R_{ct} - R_{ct}{}^{\circ}}{R_{ct}}\right) \times 100 \qquad \textbf{Eqn.5}$$

Where $\mathbf{R_{ct}}$ and $\mathbf{R_{ct}}^{\circ}$ are polarization resistance in the presence and absence of inhibitor respectively.

### *2.4. Computational studies*

On the basis of the findings of an experimental study on methionine and its derivatives by electrochemical methods, we found it useful and very interesting to undertake a quantum study of these compounds, to establish a relationship between its structures and its inhibitory efficiency. Each compound focuses on the descriptions that best describe its anti-corrosion character.

The Dmol3 module included in the Biovia Materials Studio software was used for DFT calculations (Yukna *et al*.,1998, Andzelm *et al*., 2001). Generalized Gradient Approximation (Berisha *et al*., 2019) employing the M11L (Peverati and Truhlar, 2012, Goerigk *et al*., 2011) and the triple-numeric quality with the polarization functions (TNP) (Daoudi *et al*., 2022) have been used for geometric optimizations. In this work, MD simulations have been done with the canonical NVT set for a simulation time of 800 ps with 1.0 fs as a time step (Chauhan *et al*., 2019). The temperature for the systems examined was 298 K by means of the Berendsen's thermostat. Herein, the COMPASSIII (Version 1.0) was used as force field to calculate all energetic components of considered system (Dagdag *et al*., 2022, Abdellattif *et al*., 2021).

Adsorption locations, energies and chemical adsorption processes were also included in this analysis. These simulations were carried out utilizing Fe(110) iso-area (three dimensions for the slab model: 27.306127× 27.306127× 47.161105 Å) under Periodic Boundary Conditions. This model featured the Fe layer, 10 chloride ions, 10 hydronium ions, 1000 $H_2O$ molecules and 1 inhibitor and a 35 vacuum layer were included in the simulation box.

## 3. Results and Discussion

### *3.1. The effect of MT concentration*

The different values obtained by the mass loss measurements of the rate corrosion and inhibitory efficiency of different concentrations are grouped in **Table 1** and schematically shown in **Figure 2**.

The present results of **Table 1**, shows that the corrosion rate decreases significantly after the addition of the three inhibitors. On the other hand, the inhibition efficiency increases with the increase of inhibitor concentration. This can be explained by the formation of an organic layer that covers the surface of the steel, which blocks the acid attack. The values of $E_w(\%)$ of $MT_1$, $MT_2$ and $MT_3$ inhibitors at 308K increases with increase in concentration up to $10^{-3}$M. So, for further studies, $10^{-3}$M was used as optimum concentration and for $10^{-3}$M concentration efficiency of $MT_1$ and $MT_2$ and $MT_3$ was

92,45%, 81,10% and 88,21%, respectively. It is also evident from **Figure 2** the performance of $MT_1$ is the best compared to the other inhibitors for the different concentrations used.

**Table 1.** The different corrosive parameters calculated by the mass loss measurements of mild steel in HCl 1 M with and without $MT_{1->3}$.

| Prod Code | Conc (M) | Corrosion rate (CR) (mg $cm^{-2}h^{-1}$) | Inhibition efficiency Ew (%) | θ |
|---|---|---|---|---|
| Blank | 1 | 0.80 | ----- | ----- |
| $MT_1$ | $1.10^{-6}$ | 0.47 | 41.67 | 0.42 |
| | $5.10^{-5}$ | 0.28 | 65.08 | 0.65 |
| | $1.10^{-5}$ | 0.21 | 73.42 | 0.73 |
| | $5.10^{-4}$ | 0.18 | 77.66 | 0.78 |
| | $1.10^{-4}$ | 0.17 | 79.24 | 0.79 |
| | $5.10^{-3}$ | 0.11 | 85.73 | 0.86 |
| | $1.10^{-3}$ | 0.06 | **92.45** | 0.92 |
| $MT_2$ | $1.10^{-6}$ | 0.52 | 35.03 | 0.35 |
| | $5.10^{-5}$ | 0.47 | 41.71 | 0.42 |
| | $1.10^{-5}$ | 0.37 | 53.78 | 0.54 |
| | $5.10^{-4}$ | 0.27 | 66.49 | 0.66 |
| | $1.10^{-4}$ | 0.22 | 71.93 | 0.72 |
| | $5.10^{-3}$ | 0.19 | 76.25 | 0.76 |
| | $1.10^{-3}$ | 0.15 | **81.10** | 0.81 |
| $MT_3$ | $1.10^{-6}$ | 0.49 | 40.90 | 0.41 |
| | $5.10^{-5}$ | 0.40 | 51.75 | 0.52 |
| | $1.10^{-5}$ | 0.34 | 59.28 | 0.59 |
| | $5.10^{-4}$ | 0.28 | 66.78 | 0.67 |
| | $1.10^{-4}$ | 0.24 | 71.45 | 0.71 |
| | $5.10^{-3}$ | 0.16 | 80.83 | 0.81 |
| | $1.10^{-3}$ | 0.09 | **88.21** | 0.88 |

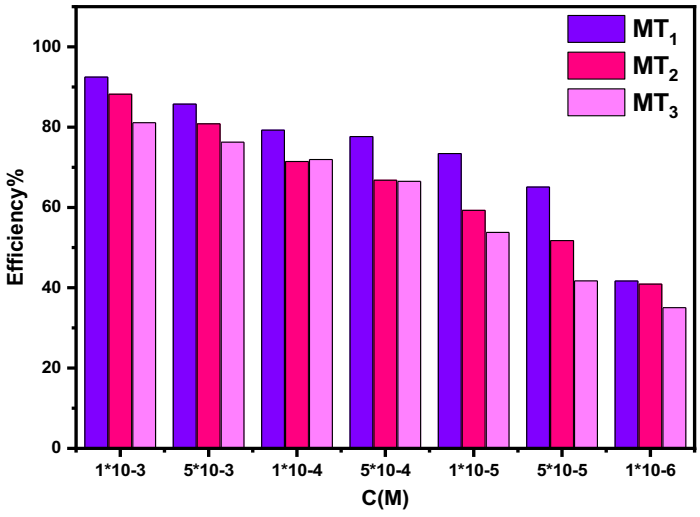


**Figure 2**. Comparison of the efficiency of $MT_{1->3}$ for different concentrations.

### *3.2. Adsorption isotherm of studied ligands*

The interaction between the inhibitor and the mild steel surface gives basic information which can be provided by the adsorption isotherm. To determine the type of adsorption isotherm corresponding to our study, different types of isotherms Langmuir, Flory-Huggins, Freundlich and Temkin were tested using their mathematical formulas equations, respectively Eqn.6-Eqn.9 (Zerfaoui *et al*., 2004, Tan *et al*., 2018, Bahlakeh *et al*., 2019, Ramezanzadeh *et al*., 2019). The experimental values obtained by the mass loss method are illustrated graphically to fit several types of adsorption isotherms (**Figure 3**)

$$\frac{C}{\theta} = C + \frac{1}{k_{ads}} \qquad \textbf{Eqn.6}$$

$$Log\left(\frac{\theta}{C}\right) = Log(k_{ads}) + xLog(1-\theta) \qquad \textbf{Eqn.7}$$

$$ln(\theta) = ln(k_{ads}) + zln(C) \qquad \textbf{Eqn.8}$$

$$\theta = -\frac{2.303logk_{ads}}{2a} - \frac{2.303logC}{2a} \qquad \textbf{Eqn.9}$$

From the graphs shown in **Figure 3**, and the $R^2$ and slope values in Table 3 are near to unity indicating that the adsorption of these inhibitors obeys Flory-Huggins and Langmuir, with a better fit of the Langmuir isotherm ($R^2$ = 0.999). This suggests that there is an interaction between adsorbed species of the inhibitor molecules on the metal surface. Langmuir equation had been derived on the assumption that no interaction exist among adsorbed inhibitor molecules. This is not true as many reports in the literature have shown that large molecules such as polymers (Umoren *et al*., 2013 & 2011) and organic molecules having polar groups (Tao *et al*., 2012) can interact by mutual repulsion or attraction (Alhaff *et al*., 2018). According to $K_{ads}$ values, the standard free energy of adsorption ($\Delta G^{\circ}_{ads}$) for $MT_1$, $MT_2$ and $MT_3$ at 35 °C were estimated by the following equation Eqn.10 (Yüce and Kardas, 2012).

$$\Delta G^{\circ}_{ads} = -RT\ ln\ (55.5 \times k_{ads}) \qquad \textbf{Eqn.10}$$

where R is the gas constant and T is the absolute temperature (K). With the value 55.5 in the above equation is equal to the concentration of water in the medium in mol/l. Calculated values of $K_{ads}$ and $\Delta G^{\circ}_{ads}$ are listed in **Table 2**.

From the results shown in Table 2, the large values of $K_{ads}$ were obtained for three studied inhibitors $MT_1$, $MT_2$ and $MT_3$ suggesting that they adsorbed easily and strongly onto the substrate surface.

However, to fully understand the types of ligand–metal bonds, it is necessary to estimate the Gibbs energy $\Delta G^{\circ}_{ads}$. Moreover, most researchers propose that for values of $\Delta G^{\circ}_{ads}$ superior to -20 kJ/mol, this energy gap corresponds to weak interactions (physical adsorption). On the other hand, when $\Delta G^{\circ}_{ads}$ is less than -40 kJ/mol, it corresponds to charge transfer between the metal surface and the inhibitor molecules by forming covalent or coordination bonds (Herrag *et al*., 2010, Zerga *et al*., 2009, Khamis *et al*., 1991). In our case, the calculated $\Delta G^{\circ}_{ads}$ values for $MT_1$, $MT_2$ and $MT_3$ were -39.87, -38.86 and -39.50 $kJmol^{-1}$, respectively at 308K; these values were between the threshold values for physical adsorption and chemical adsorption, indicating that the adsorption process of these inhibitors at mild steel surface involves both the physical as well as chemical adsorption (mixed) (Hegazy *et al*., 2015). The negative values of $\Delta G^{\circ}_{ads}$ indicate that the adsorption process is spontaneous in nature.

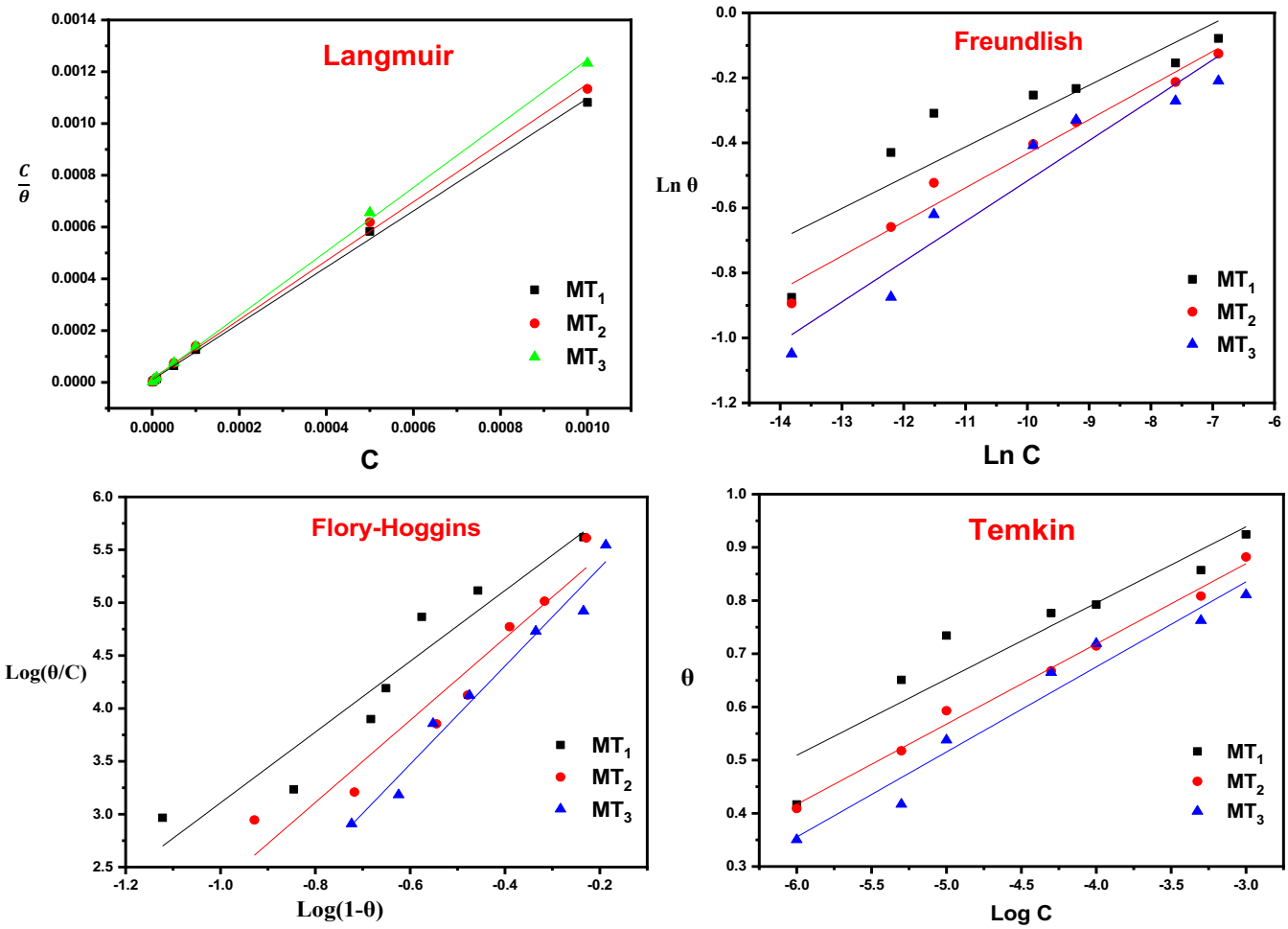


**Figure 3**. Adsorption isotherms of the MT inhibitors on the steel surface at 308K.

**Table 2 :** Different values of the $K_{ads}$ constant and $\Delta G^{\circ}_{ads}$ of the adsorption energy calculated for $MT_1$, $MT_2$ and $MT_3$ at 308K.

| Isotherm | Compound | Linear correlation | Slope | $K_{ads}$ ($M^{-1}$) | $\Delta G^{\circ}_{ads}$(KJ /mol) |
|---|---|---|---|---|---|
| **Langmuir** | *$MT_1$* | 0.9984 | 1.0877 | $1.04.10^5$ | -39.87 |
| | $MT_2$ | 0.9977 | 1.1383 | $7.02.10^4$ | -38.86 |
| | $MT_3$ | 0.9990 | 1.2358 | $9.02.10^4$ | -39.50 |
| **Flory-Huggins** | *$MT_1$* | 0.9057 | 3.3466 | 0.15 | -5.51 |
| | $MT_2$ | 0.9234 | 3.8861 | 0.16 | -5.60 |
| | $MT_3$ | 0.9671 | 4.6448 | 0.16 | -5.59 |
| **Freundlich** | *$MT_1$* | 0.7665 | 0.0947 | 1.59 | -11.47 |
| | $MT_2$ | 0.9707 | 0.1049 | 1.62 | -11.52 |
| | $MT_3$ | 0.9159 | 0.1241 | 1.38 | -11.11 |
| **Temkin** | *$MT_1$* | 0.8594 | 0.1432 | 0.73 | -9.48 |
| | $MT_2$ | 0.9914 | 0.1509 | 0.76 | -9.57 |
| | $MT_3$ | 0.9516 | 0.1599 | 0.76 | -9.58 |

### *3.3. Electrochemical study*

#### *3.3.1. Potentiodynamic polarization tests (PDP)*

The Tafel polarization curves of $MT_1$, $MT_2$ and $MT_3$ inhibitors for the mild steel in 1M of HCl solution at 308 K temperature in the absence and presence of optimum concentration $10^{-3}$M of inhibitors are represented in **Figure 4** and obtained corrosion parameters (corrosion current density, corrosion

potential, efficiency and the anodic and cathodic Tafel slopes) are recorded in **Table 3** using Ec-lab software. Addition of the inhibitors is seen to affect the anodic (metal dissolution) aswell as the cathodic (hydrogen evolution) partial reactions, shifting the corrosion potential ($E_{corr}$) slightly towards more positive (anodic) values and reducing the anodic and cathodic current densities and the corresponding corrosion current density ($i_{corr}$). This indicates that the three inhibitors functioned as mixed-type inhibitors in 1M HCl solution (Cao, 1996).

**Table 3.** Electrochemical parameter for mild steel in 1M HCl solution in the presence or absence of the optimum concentration of inhibitor at 303 K.

| Medium | C(M) | - $E_{corr}$ (mV/ECS) | - $\beta_c$ (mV/dec) | $\beta_a$ (mV/dec) | $i_{corr}$ (mA/cm$^2$) | $\eta_{EIS}$ (%) |
|---|---|---|---|---|---|---|
| **Blank** | 1 | 450.14 | 273.30 | 237.10 | 2.69 | ---- |
| **$MT_1$** | $10^{-3}$ | 453,82 | 144,60 | 73,80 | 0.13 | **95.20** |
| **$MT_2$** | $10^{-3}$ | 426.50 | 152.20 | 89.00 | 0.16 | **94.14** |
| **$MT_3$** | $10^{-3}$ | 441.06 | 183.70 | 112.00 | 0.30 | **88.92** |

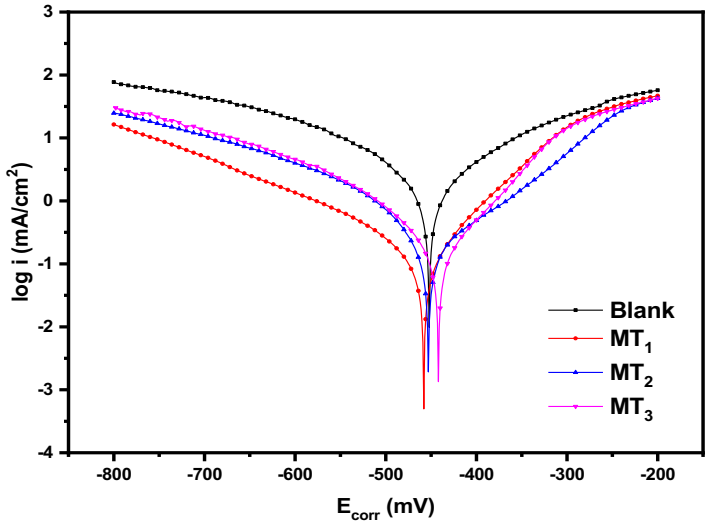


**Figure 4.** Tafel polarization plots of $MT_1$, $MT_2$ and $MT_3$ inhibitors in absence and presence of optimum concentration $10^{-3}$ at 308K.

The reduction in the value of corrosion current density in the presence of $MT_1$ inhibitor is more pronounced than $MT_2$ and $MT_3$, which results in increase in inhibition efficiency. The inhibitor molecules are first adsorbed on the mild steel surface, blocking the available reaction sites, and decrease the corrosion current density. This result is in agreement with that of gravimetric measurements. Again, it is noticed from **Table 3** that there is notable changes in both the anodic and cathodic Tafel slopes in the presence of inhibitors relative to the blank, no definite trend is seen. This observation coupled with the fact that both anodic and cathodic current densities are reduced suggests that the three inhibitor $MT_1$, $MT_2$ and $MT_3$ function as a mixed type corrosion inhibitors (Pradeep-Kumar *et al*., 2015). For comparison, the inhibition efficiency values can be classified as follows: $MT_1$ (95.20%) > $MT_3$(94.14%) > $MT_2$(88.92%). $MT_1$ showed good corrosion protection of mild steel in the aggressive solution studied (1M HCl). This indicates the powerful adsorption of the very strong sulfur structure of L-methionine leading to a higher inhibition efficiency 95.20%, compared to methionine

sulfone and methionine sulfoxide which the sulfur of L-methionine has been oxidised to the corresponding sulfone and sulfoxide which introduces a decrease in inhibition efficiency.

### *3.3.2. Electrochemical impedance spectroscopy tests (EIS)*

In this study, in order to confirm the obtained results from the polarization curves and acquire more information on the kinetics of the electrochemical processes at the mild steel/acid interface and how this is modified by the presence of inhibitor, electrochemical impedance spectroscopy was employed. The Nyquist plots for the three inhibitors are shown in **Figure 5.** The Nyquist curves show a single capacitive loop, suggesting presence of single time constant and imperfect semicircle at high frequencies, suggesting porous heterogeneous surface of mild steel and inhibitor adsorption resulting from the frequency dispersion (Yousefi *et al*., 2015).

**Figure 5** exhibits Nyquist diagram reflecting the effect of the optimum concentration $10^{-3}$ of the three inhibitors $MT_1$, $MT_2$ and $MT_3$ on the corrosion of mild steel in HCl medium 1 M at 308 K. The extracted parameters from the electrochemical graphs are grouped together in Table 4. Using the EC-Lab software, the equivalent electrical circuit was obtained and it's illustrated in **Figure 6**.

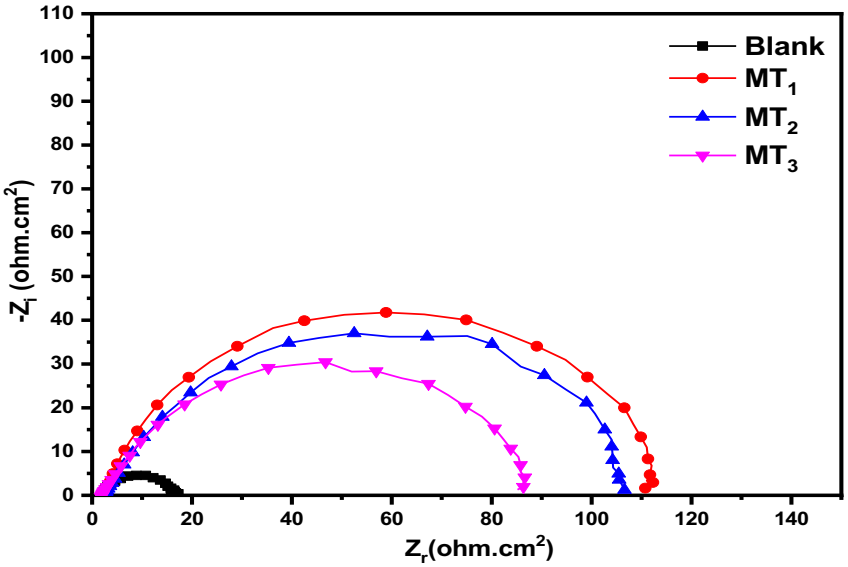


**Figure 5.** Nyquist plot for the MS in 1M HCl and with the absence and presence of $MT_1$, $MT_2$ and $MT_3$ inhibitor at 308K temperature for the optimum concentration $10^{-3}$M.

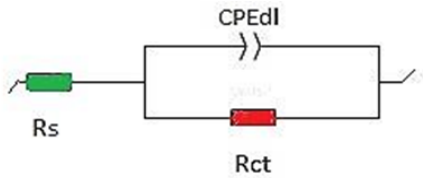


**Figure 6.** Circuit for fitting the Nyquist plot.

The equivalent circuit includes the solution resistor ($R_s$) and a bias resistor ($R_{ct}$), positioned in parallel with the constant phase element (CPE). The double layer capacitance ($C_{dl}$) was calculated from **Eqn.10** (Saraswata *et al*., 2020):

$$C_{dl} = (Y_0 R_{ct}^{n-1})^{1/n} \qquad \textbf{Eqn.10}$$

Where, $Y_0$ is the CPE constant and n is its exponent.The diagrams generate an increase in loop diameters with added $MT_1$, $MT_2$ and $MT_3$.

These kinds of results could be explained by the charge transfer resistance (Rct) increases at the interface of electrode-electrolyte solution due to adsorption of inhibitor molecules on the mild steel surface. This reflects the influence of the inhibitor on the corrosion process (Abdallah *et al*. 2016). The values recorded in **Table 4** clearly show that there is a significant increase in the charge transfer resistance $R_{ct}$ with addition of $MT_1$, $MT_2$ and $MT_3$ inhibitor at optimum concentration $10^{-3}$M, this increase is due to the replacement of the water molecules by the organic molecules adsorbed at the interface which generate the formation of a protective layer on the surface of the steel.
However, we notice the decrease of the capacity of the double layer $C_{dl}$ with the addition of the studied molecules, indicating a growth of the thickness of the double layer and the reduction of the active metal surface (Lgaz *et al.*, 2017). However, the values of parameter n are between 0.7322 and 0.8543. These results suggested an increase in the heterogeneity that reflects the adsorption of ligands at the electrode–electrolyte interface.

**Table 4.** Electrochemical parameters and corrosion inhibitory efficiency of steel in HCl (1M) without and with addition of optimum concentration of $MT_1$, $MT_2$ and $MT_3$ at 308 K.

| Prod code | Conc.(mol/l) | Rt(Ω.cm$^2$) | CPE component | | $C_{dl}$ (µF.cm$^{-2}$) | Efficiency(%) |
|---|---|---|---|---|---|---|
| | | | $Y_0$ (µF.cm$^{-2}$) | n | | |
| **Blank** | 1 | 11.17 | 501.8 | 0.7322 | 179.4 | ---- |
| **$MT_1$** | $10^{-3}$ | 113.4 | 112.7 | 0.8543 | 57.26 | 90.23 |
| **$MT_2$** | $10^{-3}$ | 108.7 | 336.9 | 0,747 | 109. 9 | 89.72 |
| **$MT_3$** | $10^{-3}$ | 85.10 | 263.3 | 0.7406 | 187 | 86.87 |

### *3.4. Effect of the temperature of the studied ligands*

The temperature is a kinetic factor strongly depends on the rate of corrosion, which suggests an important effect on the phenomenon of corrosion, as several changes intervene such as the desorption of the inhibitor and the decomposition of the inhibitor in solution when a reaction in an inhibited solution occur. On the other hand, the rise in temperature is due to desorption of adsorbed inhibitor layer on MS surface at higher temperature.In this work, the influence of temperature on the corrosion inhibitive behavior of the three tested inhibitors were investigated by weight loss measurements in the temperature range 293–333K, with and without presence of the MT inhibitors at the concentration $10^{-3}$M. It is clear from the **Table 5** that the inhibition efficiency decreased with increasing temperature.

**Table 5.** Corrosion rate and inhibition efficiency of mild steel in 1 M HCl in the absence and presence of inhibitors at different temperatures.

| T(K) | Blank | | $MT_1$ | | $MT_2$ | | $MT_3$ | |
|---|---|---|---|---|---|---|---|---|
| | 1M | | $10^{-3}$M | | $10^{-3}$M | | $10^{-3}$M | |
| | CR(mg/cm$^2$.h) | $E_w$(%) | CR(mg/cm$^2$.h) | $E_w$(%) | CR(mg/cm$^2$.h) | $E_w$(%) | CR(mg/cm$^2$.h) | $E_w$(%) |
| 293 | 1.22 | --- | 0.09 | **92.76** | 0.13 | **89.41** | 0.21 | **83.00** |
| 303 | 2.01 | --- | 0.26 | 87.09 | 0.51 | 74.58 | 0.57 | 71.79 |
| 313 | 3.14 | --- | 0.56 | 82.01 | 0.93 | 70.42 | 1.35 | 56.87 |
| 323 | 4.80 | --- | 1.05 | 78.20 | 2.42 | 49.79 | 2.77 | 42.51 |
| 333 | 7.59 | --- | 2.70 | 64.39 | 4.74 | 37.56 | 6.22 | 17.98 |

This concentration for which the inhibitory efficiency reaches a maximum value during 1h. Such type of behavior can be described on the basis that the increase in temperature leads to a shift of the

equilibrium constant towards desorption of the inhibitor molecules at the surface of mild steel (Fragoza-Mar *et al*., 2012). The inhibition efficiency of $MT_1$ is greater than $MT_2$ and $MT_3$ at all temperatures.

### *3.5. The thermodynamic parameters of activation*

To evaluate the adsorption and thermodynamic activation parameters of corrosion processes of mild steel in1M HCl solution such as activation energy, enthalpy and entropy, weight loss measurements were carried out in the temperature range 293– 333 K in the absence and presence of inhibitors. To access the value of the activation energy ($E_a$) relative to the corrosion process in the absence and presence of the inhibitor, several researchers have used the Arrhenius equation according to the following Arrhenius relation (Noor *et al*., 2008).

$$\ln W_{corr} = lnA - \frac{E_a}{RT} \qquad \textbf{Eqn.11}$$

Where $E_a$ is the activation energy, R is the perfect gas constant, A is a pre-exponential factor, T is the absolute temperature and $W_{corr}$ is the corrosion rate. **Figure 7** presents the Arrhenius plot of ln $W_{corr}$ against 1000/T for the corrosion of mild steel in 1M HCl solution in the absence and presence of inhibitors $MT_1$, $MT_2$ and $MT_3$. From **Figure 7**, the activation energy was calculated using the expression $E_a = -(\text{slope}) \times R$. The calculated values of $E_a$ are summarized in **Table 6**. It is evident from this Table that the value of activation energy for inhibitor containing solution is higher as compared to the 1M HCl solution, indicating that the dissolution of mild steel was decreased due to formation of a barrier by the adsorption of the inhibitors on metal surface (Dehri *et al*., 2006).

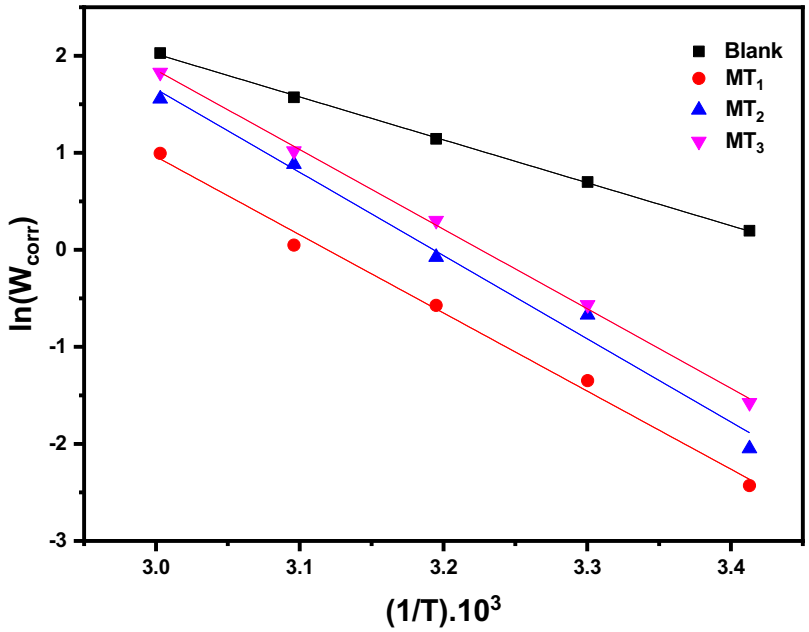


**Figure 7.** Arrhenius lines plotted from the gravimetric method of steel in 1 M HCl without and with MT $10^{-3}$M

Also, the values of enthalpy ($\Delta H_a$) and entropy of activation ($\Delta S_a$) are calculated from extrapolation of the Ln (W/T) plot as a function of the inverse of temperature (**Figure 8**) with a slope equal to ($-\Delta H_a/R$) and the intersection with the ordinate axis equal to ( Ln (R/Nh)+$\Delta S_a/R$) using the Arrhenius transition **Eqn.12**:

$$Ln\left(\frac{Wcorr}{T}\right) = [Ln\left(\frac{R}{Nh}\right) + (\frac{\Delta S_a^\circ}{R})]\text{-}\frac{\Delta H_a^\circ}{RT}$$ **Eqn.12**

h: Planck's constant, N: Avogadro number, $\Delta H_a^\circ$: activation enthalpy of and $\Delta S_a^\circ$: activation entropy.

From the results shown in **Table 6**, it is notably that the parameters ($\Delta H_a^\circ$ ,$\Delta S_a^\circ$) of mild steel in the presence of MTs inhibitors are higher compared to the uninhibited solution.

The positive enthalpy values $\Delta H_a^\circ$ indicate the endothermic dissolution process of the steel (Mu *et al*., 2004). Moreover, the negative value of $\Delta S_a^\circ$ for three inhibitors indicates that the formation of the activated complex in the rate determining step represents an association rather than a dissociation step, meaning that a decrease in disorder takes place during the course of the transition from reactants to activated complex (Wang *et al*., 2011). On the other hand, we notice that the activation energy $E_a$ and enthalpy $\Delta H_a^\circ$ vary with concentration in the same way verifying the following thermodynamic relation **Eqn.13** (Stern *et al*., 1957):

$$E_a\text{-}\Delta H_a^\circ = RT = cte$$ **Eqn.13**

**Table 6.** Thermodynamic activation parameters of steel in HCl without and with $10^{-3}$M of $MT_1$, $MT_2$ and $MT_3$.

| Compound | C (M) | K (mg /cm$^2$.h) | $E_a$ (kJ.mol$^{-1}$) | $\Delta H_a^\circ$ (kJ mol$^{-1}$) | $\Delta S_a^\circ$ (J mol$^{-1}$) | $E_a^\circ$-$\Delta H_a^\circ$ |
|---|---|---|---|---|---|---|
| **Blank** | 1 | $4.37.10^6$ | 36.78 | 34.18 | -126.49 | 2.59 |
| **$MT_1$** | $10^{-3}$ | $8.11.10^{10}$ | 66.95 | 64.36 | -44.77 | 2.59 |
| **$MT_2$** | $10^{-3}$ | $3.07.10^{11}$ | 68.17 | 65.57 | -33.69 | 2.59 |
| **$MT_3$** | $10^{-3}$ | $7.81.10^{11}$ | 71.30 | 68.70 | -25.94 | 2.59 |

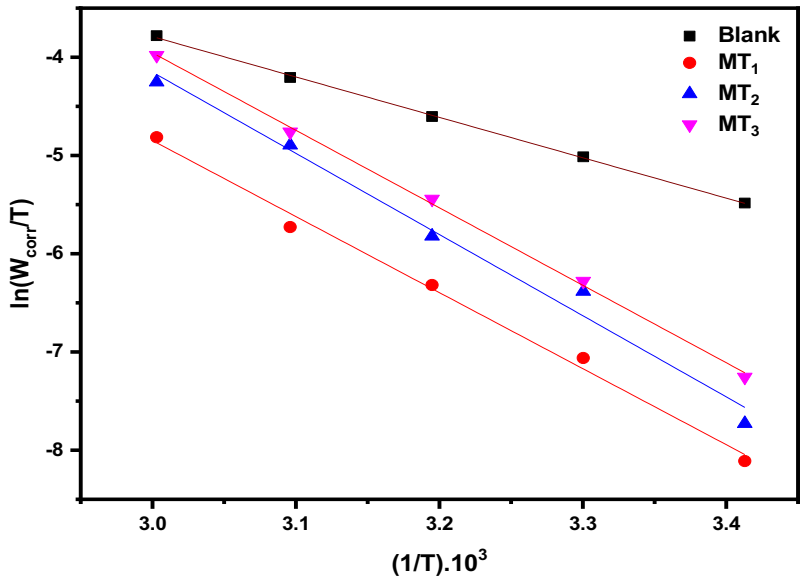


**Figure 8.** Arrhenius transition lines of mild steel in 1 M HCl without and with MT $10^{-3}$M

### *3.6. Theoretical analysis*

#### *3.6.1. DFT results*

**Figure 9** shows the σ-profile of the MT1, MT2 and MT3 molecules. The selected inhibitors have good H-bonding acceptor and donor sites, which are responsible for the physical and chemical adsorption mechanisms. The accepting and donating abilities of the MT1, MT2 and MT3 molecules depend on the interaction between their functional groups and $H_2O$ molecules.

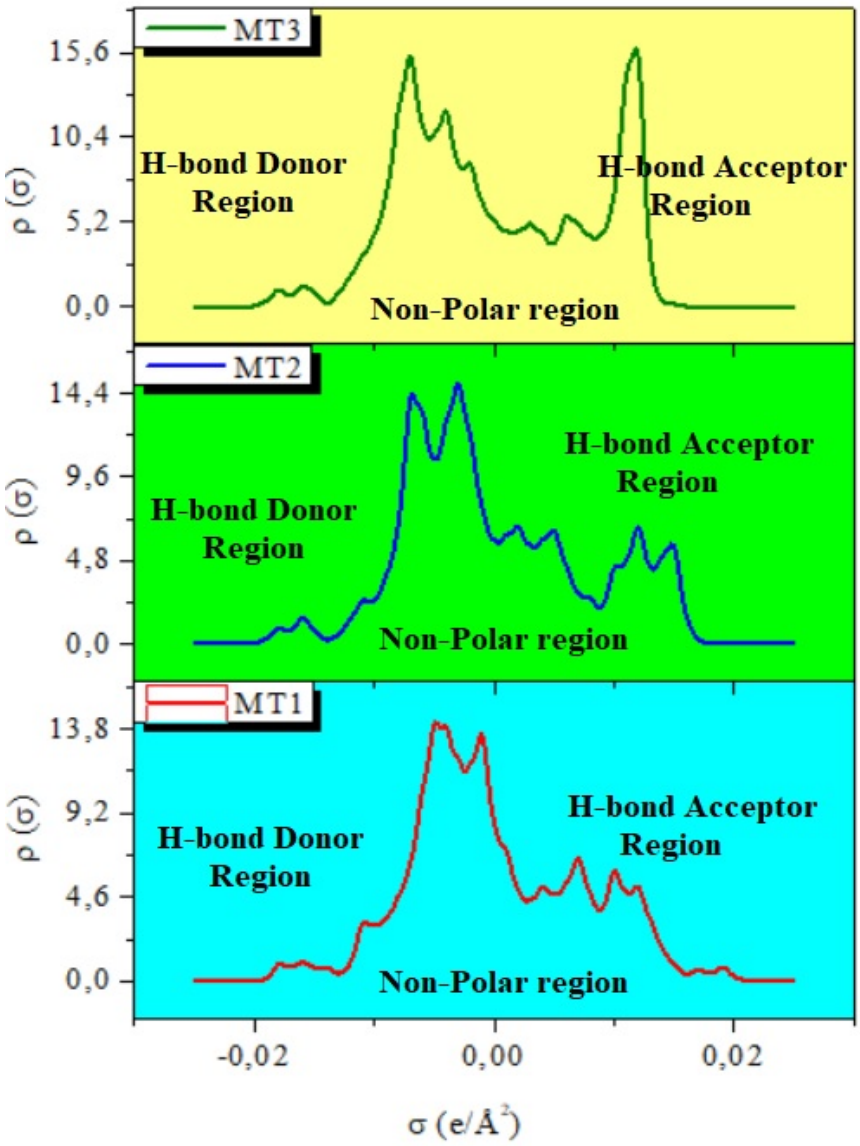


**Figure 9.** Charge density profiles (σ) of the MT1, MT2 and MT3 molecules.

Mulliken charges related to the vibrational properties of the molecule assess how atomic displacement affects the charge of the electronic structure. The negatively charged heteroatom presents the active adsorption site on the metal surface. The process is carried out by a donor-acceptor type reaction.

It has been reported that the higher the atomic charges of the adsorbed centre are negative, the more easily the atom abandons its electrons in the orbital vacuum of the metal (Berisha *et al*., 2021, Mehmeti, 2022, Oukhrib *et al*., 2021, Damej *et al*., 2022). The distribution of Mulliken Atomic Charges (MAC) is schematized by **Figure 10**. Nitrogen and oxygen atoms can be seen to have high charge densities. Regions with greater electron densities are usually sites through which electrophiles can attack. Therefore, N and O are the active centers that have the greatest bonding capacity at the metal surface. Further, sulfur atoms carry positive charges, and are sites through which nucleophiles can attack. So, the MTs can accept steel electrons through these atoms.

From **Figure 10**, negative charges can be seen to be found in the following volumes: O (-0.765), N (-0.918) and the most negative atom is O in red O (-0.934) for the compound: MT1; O (-0.756), O (-0.942), N (-0.914) and the most negative atom O (-1.111) for the compound: MT2 and O (-1.118), O (-0.952), O (-0.759), N (-0.914) and the most negative atom O (-1.121) for compound MT3.

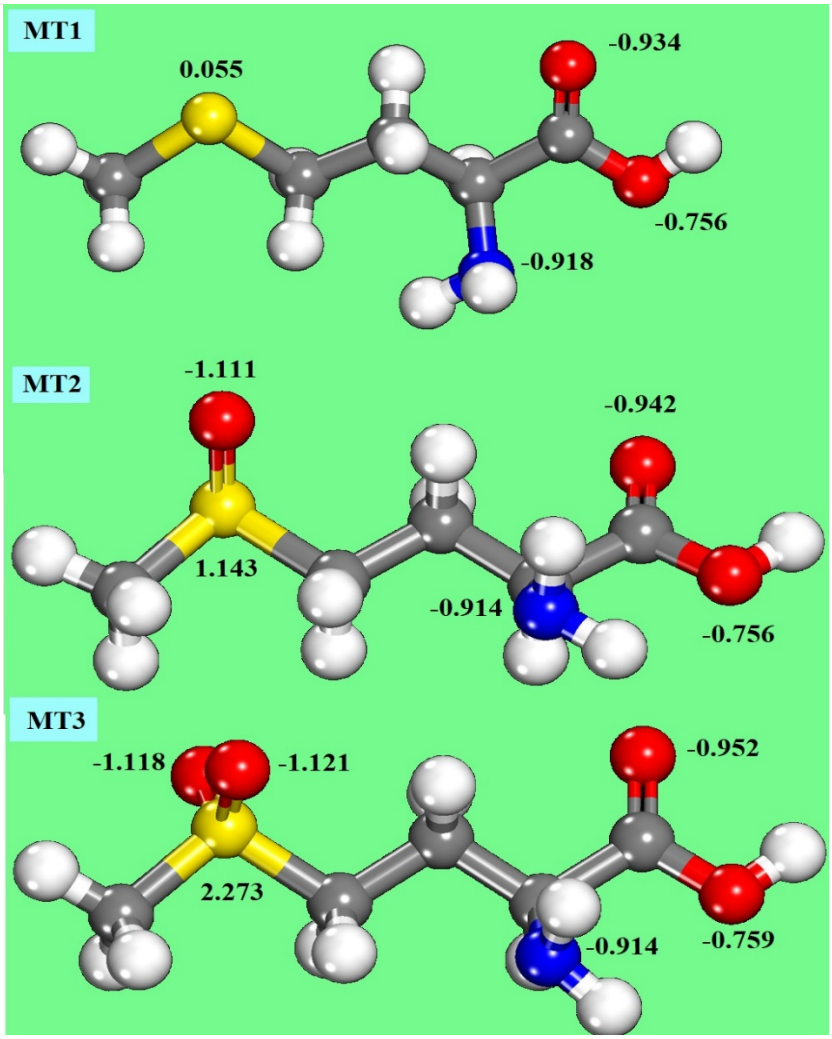


**Figure 10.** Distribution of the MAC values O, N and S atoms of MT1, MT2 and MT3 molecules.

In order to give a better overview of the experimental results, different quantum parameters namely $E_{HOMO}$, $E_{LUMO}$ and the energy difference between HOMO-LUMO ($\Delta E = E_{HOMO} - E_{LUMO}$) of t the molecules used are calculated to find a link between the parameters structural properties of MT1, MT2 and MT3 inhibitors and the anti-corrosive properties of iron in an acidic environment. **Table 7**, presents the calculated quantum chemical parameter values for the compounds MT1, MT2 and MT3.

By definition, $E_{HOMO}$ is often related to the molecule's ability to give electrons. A high HOMO energy value facilitates the molecule's tendency to give electrons to species accepting electrons with unoccupied molecular orbits with a low energy level (Daoudi *et al*., 2023, Iroha *et al.*, 2023). Instead, $E_{LUMO}$ shows the molecule's capacity to receive electrons (Ganjoo *et al*., 2022). A low value of $E_{LUMO}$ indicates that the molecule certainly accepts electrons. $\Delta E$ is the minimal energy required for the excitation of an electron in a molecule (Daoudi *et al*., 2022). Consequently, the value of $\Delta E$ provides a measure of the stability of the compound formed on the metal surface (Chile *et al*., 2022).

The analysis of the findings in Figure 11 shows that the $\Delta E$ value of MT1 (4.616 eV) is lower than that of MT2 (5.324 eV) and MT3 (5.575 eV). This indicates that MT1 has a strong ability to share electrons with the metal to establish coordination bonds by promoting the process of chemisorption of the inhibitor at the surface of the iron under study (Benali *et al*., 2007). The $\Delta N$ values are correlated to the inhibition efficiency resulting from electron transfer. A decrease in $\Delta N$ indicates a reduction in the inhibitor's electron donation power on the metallic surface. According to Lukovits et al, if $\Delta N < 3.6$, inhibitory efficiency increases as the ability to give electrons to the metal surface increases (Dagdag *et*

*al*., 2020). The values of ΔN are positive and less than 3.6 thus confirming that the three inhibitors can donate electrons to the metal to generate bonds and consequently lead to the formation of adsorbed stable inhibiting layers limiting corrosion.

**Table 7.** Theoretical parameters calculated for MT1, MT2 and MT3 inhibitors.

| **Theoretical parameters** | **MT1** | **MT2** | **MT3** |
|---|---|---|---|
| **I (eV)** | 5.498 | 6.105 | 6.349 |
| **A (eV)** | 0.882 | 0.781 | 0.774 |
| **χ (eV)** | 3.190 | 3.443 | 3.561 |
| **η (eV)** | 2.308 | 2.662 | 2.787 |
| **σ ($eV^{-1}$)** | 0.433 | 0.375 | 0.358 |
| **ΔN** | 0.825 | 0.668 | 0.617 |
| **$\Delta E_{back\text{-}donation}$** | -0.577 | -0.665 | -0.696 |

The Optimized structures, LUMO, HOMO and ESP pictures of MT1, MT2 and MT3 of molecules are shown in the **Figure 11**. It is thus observed that for the three inhibitory molecules, the HOMO electron density is distributed on dimethyl sulfane (MT1), (methylsulfinyl) methane (MT2) systems and for the MT3 compound over the glycine function. For the LUMO electron density is distributed over the sulfur and glycine function (MT1), glycine function (MT2) systems and for the MT3 compound over the glycine function.

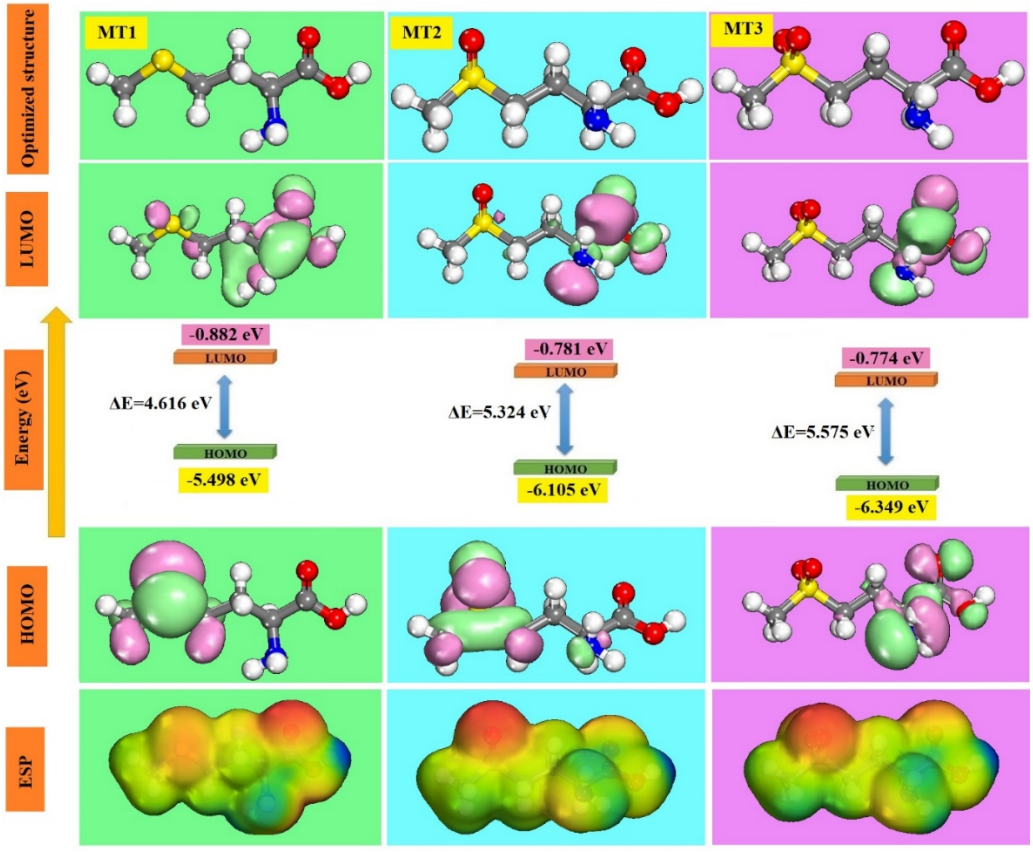


**Figure 11.** Optimized structures, LUMO, HOMO and ESP pictures of MT1, MT2 and MT3 molecules.

We can see that electron density from the location of HOMO and LUMO has been distributed almost over a part of each molecule, thanks to the presence of the nitrogen, oxygen and sulfur atoms comprising several n electrons in the chemical structures MT1, MT2 and MT3. Thus, the unoccupied orbital (d) of the iron atom can accept electrons from the molecules for the inhibitors to form a coordination gap. In addition, the three inhibitors can accept electrons from the iron atom with its anti-link orbits to form a backward binding loop. We used the molecular electrostatic potential (ESP) (**Figure 11**) to determine the sites of electrophilic and nucleophilic reactions. The electron density regions mapped with the ESP on the optimized geometry of the inhibitors are obtained. The electrophilic areas are bounded by the red and yellow colors of the ESP map while the light blue and blue colors indicate the nucleophilic active ranges (Dagdag *et al.* 2022- Dagdag *et al.*, 2017, Haldhar *et al.*, 2021) . For the three inhibitors, it can be seen that the electron-rich regions are localized around the heteroatoms (oxygen, nitrogen and sulphur). It is the active sites that give nucleophilic reactions in the corrosion inhibition process.

### *3.6.2. MD and MC simulations*

The MD and MC simulations results adsorption configurations and positions of the studied inhibitory molecules MT1, MT2 and MT3 inhibitors on the Fe(110) substrate are presented in **Figure 12**.

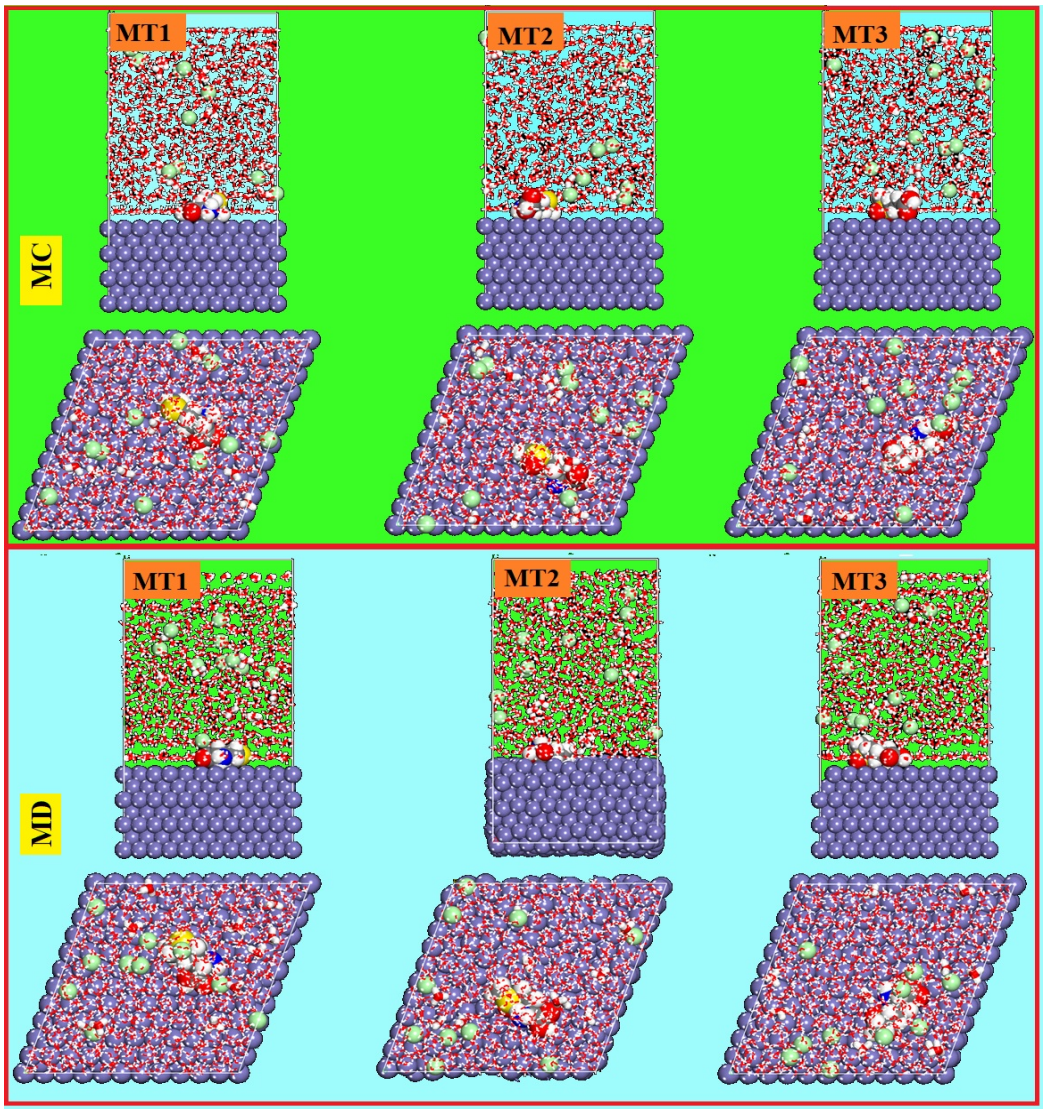

**Figure 12.** MD and MC simulations results adsorption configurations and positions of the $MT_1$, $MT_2$ and $MT_3$ inhibitors forms.

It is observed in **Figure 12**, that the inhibitor molecules are adsorbed with a position almost parallel to the plane of the metal surface. From these configurations, it can be concluded that the most significant interactions (chemisorption) are the interactions involving the Fe atoms with the oxygen and nitrogen atoms of the inhibitors with a maximum distance less than 3.5 Å for the MT1, MT2 and MT3 inhibitors considering that the physical interactions between inhibitory molecules and iron atoms induced by the dispersal forces of Van der Waals, may be contributed to the attraction of the net molecule surface (Abdellattif *et al*., 2021, Dagdag e*t al*., 2021). The adsorption energies ($E_{ads}$) are calculated and then represented in **Figure 13**. For the distribution of the $E_{ads}$ for the MT1, MT2 and MT3 inhibitors forms onto the Fe(110) substrate in 1M HCl medium by MC simulations. According these results, the absolutes values of $E_{ads}$ can be classified according to the following order:

**MT3 (-130.55 kcal/mole) > MT2 (-106.45 kcal/mole) > MT1 (-95.45 kcal/mole).**

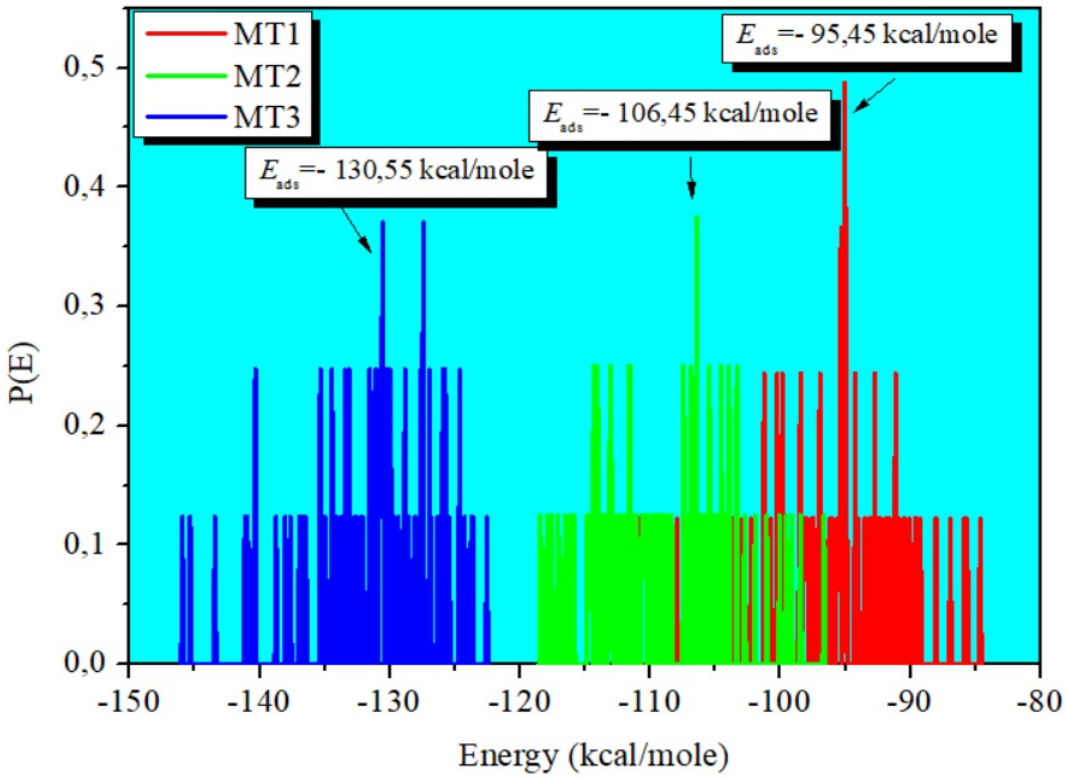


**Figure 13.** Distribution of the $E_{ads}$ of the MT1, MT2 and MT3 inhibitors via MC simulation.

RDF is an appropriate calculation tool for estimating estimate the length of bond between the adsorbed inhibitor molecule and the target surface. It is well known that the inter-atomic distance from 1.0 to 3.5 Å is usually associated with the chemical bond, whereas the non-binding one (i.e. physical interaction) corresponds to a distance greater than 3.5 Å (Srivastava *et al*., 2017, Singh *et al*., 2018). In our case, **Figure 14** summarizes the distance between iron atoms and N, O and S atoms of the MT1, MT2 and MT3 inhibitors. These represent the highest peak of RDF curves. As illustrated in the Figure 14, except Fe–O (3.03 Å) for MT1, Fe–O (2.93 Å) for MT2, Fe–O (2.93 Å) for MT3, Fe–N (3.09 Å) for MT1, Fe–N (4.59 Å) for MT2, Fe–N (3.07 Å) for MT3, most inter-tomic distances are less than 3.5 Å, indicating that chemical binding can occur between the MTs compounds tested and the protected surface.

However, almost these distances are smaller for the MT1 inhibitor. This suggests high adsorption of MT1 over the metallic surface compared to MT2 and MT3.

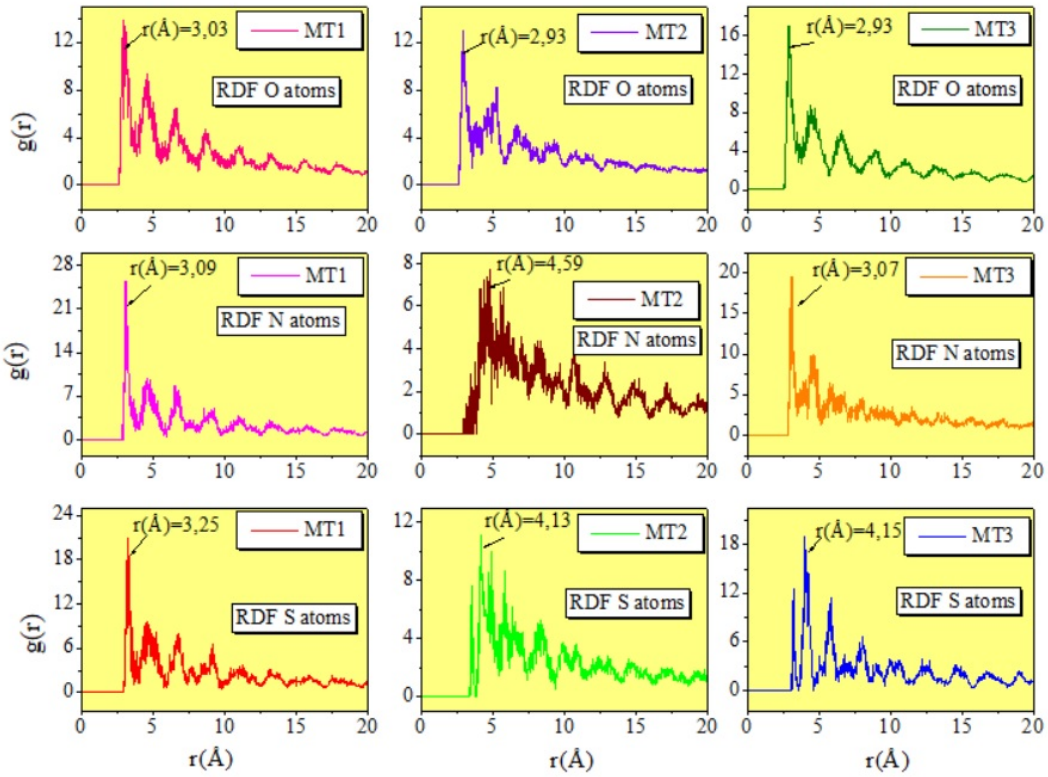


**Figure 14.** RDF of the O, N and S atoms of the MT1, MT2 and MT3 inhibitors, obtained via MD.

### *3.7. Mechanism of MTs adsorption*

The corrosion inhibition of mild steel in hydrochloric acid solution by different inhibitors (MT1, MT2 and MT3) can be justified on the grounds of molecular adsorption. The adsorption mechanism proposal of MT1 ligand on the MS metal surface of the optimum inhibitor (MT1) in a corrosive medium is shown in **Figure 15**.

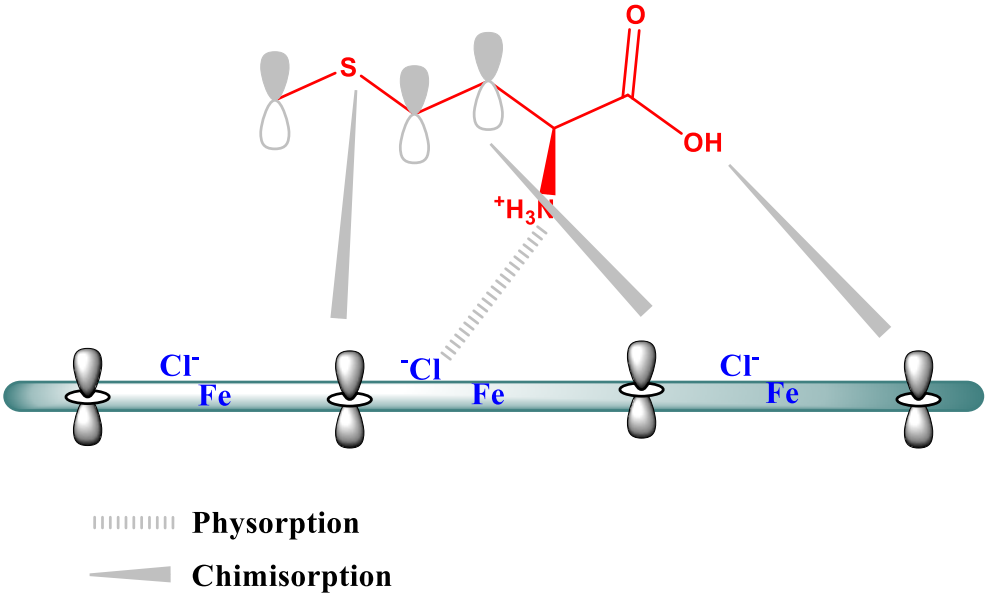


**Figure 15.** Adsorption mechanism proposal of MT1 ligand on the MS metal surface

The adsorption of an amino acids inhibitor cannot be considered as just physical or only chemical. The value of Gibb's free energy ($\Delta G^{\circ}_{ads}$) proposes that adsorption of MTs molecules evolves both physical and chemical adsorptions. In acidic solutions these inhibitors exist as protonated species. In the three inhibitors the nitrogen atoms present in the molecules can be easily protonated in acidic solution and convert into quaternary compounds. The MTs molecules get physically adsorbed by electrostatic force between protonated species and a mild steel surface and decreased the evolution of hydrogen. It is well known that mild steel becomes positive charged in 1 M HCl with respect to the potential of zero charge (PZC) (Deng *et al*., 2011). Moreover, after the liberation of hydrogen, the heteroatoms return to their neutral form. The chemical adsorption of the MTs molecules on mild steel surface takes place via donor–acceptor interaction between lone electron pairs of heteroatoms (oxygen, nitrogen and sulphur) with the vacant ''d" orbitals on the metal surface (El Ibrahimi *et al*., 2020).

## Conclusion

In the progress of this work, $MT_1$, $MT_2$ and $MT_3$ act as efficient corrosion inhibitor and $MT_1$ has higher corrosion inhibition efficiency than MT2 and MT3. Weight loss study suggested that $MT_1$, $MT_2$ and $MT_3$ inhibitors offer 92,45%, 88,21% and 81,10% inhibition efficiency at $10^{-3}$ M concentration and 303K temperature. Specifically, from the Tafel curves, it was shown that MTs act as mixed-type inhibitors. Furthermore, the thermodynamic adsorption parameters for corrosion inhibition showed that these inhibitors impede corrosion by spontaneous chemical and physical adsorption on the metal surface. In addition, the measurements extracted from Nyquist diagram showed that the charge transfer resistance increases with the increase of the concentration of each inhibitor. On the other hand, the double layer capacity decreases due to the adsorption of the compounds on the steel surface through the formation of a protective layer of acid solution. Also, the tested compounds on the steel surface are adsorbed according to the Langmuir isotherm. Additionally, this study was validated by quantum methods. The results of this research represent a better understanding of the functional properties of the studied inhibitors.

**Disclosure statement:** *Conflict of Interest:* The authors declare that there are no conflicts of interest.
*Compliance with Ethical Standards:* This article does not contain any studies involving human or animal subjects.

## References


Aatiaoui A. (2023) Synthesis, characterization, and corrosion inhibition activity of new imidazo [1.2-a] pyridine chalcones, *Materials Science and Engineering: B*, 290, 116287

Abdallah M., Altass H.M., Al-Gorair A.S., Al-Fahemi J.H., Jahdaly B.A.A.L., Soliman K.A., (2021). Natural nutmeg oil as a green corrosion inhibitor for carbon steel in 1.0 M HCl solution: Chemical, electrochemical, and computational methods, *J. Mol. Liq.,* 323, 115036. 10.1016/j.molliq.2020.115036

Abd El-Lateef H.M., Shalabi K., Tantawy A.H. (2020). Corrosion inhibition and adsorption features of novel bioactive cationic surfactants bearing benzenesulphonamide on C1018-steel under sweet conditions: combined modeling and experimental approaches, *J. Mol. Liq.,* 320, 114564. 10.1016/j.molliq.2020.114564

Abdellattif M. H., Alrefaee S. H., Dagdag O., Verma C., and Quraishi M. (2021) Calotropis procera extract as an environmental friendly corrosion Inhibitor: Computational demonstrations, *Journal of Molecular Liquids*, 337, 116954

Abdallah Z.A., Ahmed M.S., Saleh M.M. (2016) Organic synthesis and inhibition action of novel hydrazide derivative for mild steel corrosion in acid solutions, *Mater. Chem. Phys.,* 174, 91–99

Alhaff M.T., Umoren S.A., Obot I.B., Ali S.A. (2018). Isoxazolidine derivatives as corrosion inhibitors for low carbon steel in HCl solution: experimental, theoretical and effect of KI studies, *RSC Adv.,* 8, 1764–1777

Andzelm J., King-Smith R., and Fitzgerald G. (2001) Geometry optimization of solids using delocalized internal coordinates, *Chemical Physics Letters,* 335(3-4), 321-326. 10.1016/S0009-2614(01)00030-6
Aouniti A., Chetouani A., Kertit S., Hammouti B., Salghi R., Bazzi L. (2022). Methionine derivatives as green corrosion inhibitors: Review, *EHEI J. Sci. Technol.* 02(2), 78-87
Aytac A., Bilgic S., Gece G., Ancin N., Oztas S.G. (2012) Experimental and theoretical study of the inhibition effects of some Schiff bases as corrosion inhibitors of aluminium in HCl, *Materials and Corrosion,* 63, 729-734. doi:10.1002/maco.201106241
Bahlakeh G., Ramezanzadeh B., Dehghani A. (2019). Ramezanzadeh M., Novel costeffective and high-performance green inhibitor based on aqueous Peganum harmala seed extract for mild steel corrosion in HCl solution: Detailed experimental and electronic/atomic level computational explorations, *J. Mol. Liq.,* 283, 174–195
Benali O., Larabi L., Traisnel M., Gengembre L., and Harek Y. (2007). Electrochemical, theoretical and XPS studies of 2-mercapto-1-methylimidazole adsorption on carbon steel in 1 M $HClO_4$, *Applied surface science,* 253, 6130-6139
Berisha A., Podvorica F. I., and Vataj R. (2021). Corrosion Inhibition Study of Mild Steel in an Aqueous Hydrochloric Acid Solution Using Brilliant Cresyl Blue–a Combined Experimental and Monte Carlo Study, *Portugaliae Electrochimica Acta,* 39, 393-401
Berisha A., (2019) Interactions between the aryldiazonium cations and graphene oxide: A DFT study, *Journal of Chemistry,* 2019 | Article ID 5126071, doi:10.1155/2019/5126071
Cao C. (1996) On electrochemical techniques for interface inhibitor research, *Corros. Sci.,* 38, 2073–2082, https://doi.org/10.1016/S0010-938X(96)00034-0
Chauhan D. S., Quraishi M. A., Sorour A. A., Saha S. K., and Banerjee P., (2019) Triazole-modified chitosan: a biomacromolecule as a new environmentally benign corrosion inhibitor for carbon steel in a hydrochloric acid solution, *RSC Advances,* 9, 14990-15003. doi:10.1039/C9RA00986H
Chetouani A., Medjahed K., Al-Deyab S.S., Hammouti B., Warad I., Mansri A., Aouniti A., (2012) Inhibition of Corrosion of Pure Iron by Quaternized Poly(4Vinylpyridine)-Graft- Bromodecane in Sulphuric Acid, *Int. J. Electrochem. Sci.,* 7 (7), 6025-6043
Daoudi W., El Aatiaoui A., Falil N., Azzouzi M., Berisha A., Olasunkanmi L. O., Dagdag O., Ebenso E. E, Koudad M., Aouinti A., Loutou M., Oussaid A. (2022) Essential oil of Dysphania ambrosioides as a green corrosion inhibitor for mild steel in HCl solution, *Journal of Molecular Liquids,* 363, 119839
Chile N. E., Haldhar R., Godffrey U. K., Chijioke O. C., Umezuruike E. A., Ifeoma O. P., Oke Oke O. O. M., Ichou H., Arrousse N., Kim S.C., Dagdag O., Ebenso E. E., Taleb M. (2022). Theoretical study and adsorption behavior of urea on mild steel in automotive gas oil (AGO) medium, *Lubricants,* 10, 157
Dagdag O., Berisha A., Mehmeti V., Haldhar R., Berdimurodov E., Hamed O., Jodeh S., Lgaz H., Sherif E.M., Ebenso E.E., (2022). Epoxy coating as effective anti-corrosive polymeric material for aluminum alloys: Formulation, electrochemical and computational approaches, *Journal of Molecular Liquids,* 346, 117886
Dagdag O., El Harfi A., El Gana L., Safi Z. S, Guo L., Berisha A., (2021) Designing of phosphorous based highly functional dendrimeric macromolecular resin as an effective coating material for carbon steel in NaCl: Computational and experimental studies, *Journal of Applied Polymer Science,* 13, 849673
Dagdag O., Safi Z., Erramli H., Wazzan N., Obot I., Akpan E., Verma C., Ebenso E.E., Hamed O., El Harfi A. , (2019). Anticorrosive property of heterocyclic based epoxy resins on carbon steel corrosion in acidic medium: Electrochemical, surface morphology, DFT and Monte Carlo simulation studies, *Journal of Molecular Liquids,* 287, 110977. Doi:10.1016/j.molliq.2019.110977
Dagdag O., Safi Z., Qiang Y., Erramli H., Guo L., Verma C., Ebenso E. E., Kabir A., Wazzan N., El Harfi A., (2020). Synthesis of macromolecular aromatic epoxy resins as anticorrosive materials: computational modeling reinforced experimental studies, *ACS omega,* 5, 3151-3164. doi:10.1021/acsomega.9b02678
Daoudi W., Azzouzi M., Dagdag O., El Boutaybi A., Berisha A., Ebenso E. E., Oussaid A., El Iroha N. B., Anadebe V. C., Maduelosi N. J., Nnanna L. A., Isaiah L. C., Dagdag O., Berisha A., Ebenso E.E., (2023) Linagliptin drug molecule as corrosion inhibitor for mild steel in 1 M HCl solution: Electrochemical, SEM/XPS, DFT and MC/MD simulation approach, *Colloids and Surfaces A: Physicochemical and Engineering Aspects,* 660, 130885
Damej M., Hsissou R., Berisha A., Azgaou K., Sadiku M., Benmessaoud M., Labjar N. , El hajjaji S. , (2022) New epoxy resin as a corrosion inhibitor for the protection of carbon steel C38 in 1M HCl experimental and theoretical studies (DFT, MC, and MD), *Journal of Molecular Structure,* 1254, 132425. doi:10.1016/j.molstruc.2022.132425

Dehri I., Ozcan M., (2006) The effect of temperature on the corrosion of mild steel in acidic media in the presence of some sulphur-containing organic compounds, *Mater. Chem. Phys.,* 98, 316–323

Deng S., Li X., Fu H., (2011) Acid violet 6B as a novel corrosion inhibitor for cold rolled steel in hydrochloric acid solution, Corros Sci., 53, 760–8

Dkhireche N., Galai M., Ouakki M., Rbaa M., Ech-chihbi E., Lakhrissi B., EbnTouhami M., (2020) Electrochemical and theoretical study of newly quinoline derivatives as a corrosion inhibitors adsorption onmild steel in phosphoric acid media, *Inorg. Chem. Commun.,* 121, 108-222. doi:10.1016/j.inoche.2020.108222

El Aatiaoui A., Daoudi W., El Boutaybi A., Guo L., Benchat N.E., Aouinti A., Oussaid A., Loutou M., (2022) Synthesis and anticorrosive activity of two new imidazo[1, 2-a]pyridine Schiff bases, Journal of Molecular Liquids, 350, 118458. doi: 10.21203/rs.3.rs-2418901/v1

El Ibrahimi B., (2020) Atomic-scale investigation onto the inhibition process of three 1,5 benzodiazepin-2-one derivatives against iron corrosion in acidic environment, *Colloid Interface Sci. Commun.,* 37, 100279

Fragoza-Mar L., Olivares-Xometl O., (2012) Domínguez-Aguilar M.A., Flores E.A., Arellanes-Lozada P., Jimenez-Cruz F., Corrosion inhibitor activity of 1,3-diketone malonates for mild steel in aqueous hydrochloric acid solution, *Corros. Sci.,* 61, 171–184

Ganjoo R., Sharma S., Thakur A., Assad H., Sharma P. K., Dagdag O., (2022). Experimental and theoretical study of Sodium Cocoyl Glycinate as corrosion inhibitor for mild steel in hydrochloric acid medium, *Journal of Molecular Liquids,* 364, 119988

Goerigk L. and Grimme S., (2011) A thorough benchmark of density functional methods for general main group thermochemistry, kinetics, and noncovalent interactions, *Physical Chemistry Chemical Physics,* 13, 6670-6688. doi:10.1039/C0CP02984J

Haldhar R., Kim S.-C., Prasad D., Bedair M., Bahadur I., Kaya S., et al., (2021) Papaver somniferum as an efficient corrosion inhibitor for iron alloy in acidic condition: DFT, MC simulation, LCMS and electrochemical studies, *Journal of Molecular Structure,* 1242, 130822

Haldhar R., Prasad D., Bahadur I., Dagdag O., Berisha A. (2021). Evaluation of Gloriosa superba seeds extract as corrosion inhibition for low carbon steel in sulfuric acidic medium: a combined experimental and computational studies, *J. Mol. Liq.,* 323, 114958. doi:10.1016/j.molliq.2020.114958

Hammouti B., Aouniti A., Taleb M., Brighli M., Kertit S. (1995), L-Methionine methyl ester hydrochlorid as corrosion inhibitor of iron in 1M HCl, Corrosion, 51 N°6, 411-416.

Hegazy M.A. (2015) Novel cationic surfactant based on triazole as a corrosion inhibitor for carbon steel in phosphoric acid produced by dihydrate wet process*, J. Mol. Liq.,* 208, 227–236

Herrag L., Hammouti B., Elkadiri S., Aouniti A., Jama C., Vezin H., Bentiss F. (2010) Adsorption properties and inhibition of mild steel corrosion in hydrochloric solution by some newly synthesized diamine derivatives: Experimental and theoretical investigations, *Corros. Sci.,* 52 (9), 3042–3051

Jose Santana J., Paehler M., Schuhmann W., Souto R.M. (2012). Chempluschem, Investigation of Copper Corrosion Inhibition with Frequency-Dependent Alternating-Current Scanning Electrochemical Microscopy, *ChemPhysChem*, 77 (8)**,** 707-712**.** doi:10.1002/cplu.201200091

Kaczerewska O., Garcia R.L., Akid R., Brycki B., (2017). Efficiency of cationic gemini surfactants with 3-azamethylpentamethylene spacer as corrosion inhibitors for stainless steel in hydrochloric acid, J. Mol. Liq., 247, 6–13. doi:10.1016/j.molliq.2017.09.103

Karthik G., Sundaravadivelu M., (2017) Experimental and theoretical studies of antiulcer drugs with benzimidazole rings as corrosion inhibitor for copper in 1 M nitric acid medium, *J. Adhes. Sci. Technol.,* 31, 530–551. doi:10.1080/01694243.2016.1222047

Kesavan D., Tamizh M.M., Gopiraman M., Sulochana N., Karvembu R., (2012). Physicochemical Studies of 4-Substituted N-(2-Mercaptophenyl)-Salicylideneimines: Corrosion Inhibition of Mild Steel in an Acid Medium, *J Surfactants Deterg* 15, 567-576. doi:10.1007/s11743-012-1338-z

Khamis E., Bellucci F., Latanision R.M., El-Ashry E.S.H., (1991) Acid Corrosion Inhibition of Nickel by 2-(Triphenosphoranylidene) Succinic Anhydride, *Corrosion*, 47, 77–686.doi:10.4236/wjm.2013.32007

Lgaz H., Salghi R., Jodeh S., Hammouti B., (2017). Effect of clozapine on inhibition of mild steel corrosion in 1.0M HCl medium, *J. Mol. Liq.,* 225, 271–280

Loukili H., Azzaoui K., Bouyanzer A., Kertit S., Hammouti B. (2022), Corrosion Inhibition using Green Inhibitors: An Overview, *Maghr. J. Pure & Appl. Sci.* 02(2), 82-93, https://doi.org/10.48383/IMIST.PRSM/mjpas-v8i1.29392

Mehmeti V. (2022). Nystatin Drug as an Effective Corrosion Inhibitor for Mild Steel in Acidic Media-An Experimental and Theoretical Study,"*Corrosion Science and Technology,* 21, 21-31

Mehta R. K., Yadav M., Obot I.B. (2022) Electrochemical and computational investigation of adsorption and corrosion inhibition behaviour of 2-aminobenzohydrazide derivatives at mild steel surface in 15% HCl, *Materials Chemistry and Physics,* 290, 126666. doi: 10.1016/j.matchemphys.2022.126666

Merimi C., Hammouti B., Zaidi K., Elmsellem H. (2023). Comparative study of inhibitory efficacy of drug (Acetaminophen) in 1 M HCl medium applied to carbon and mild steels, *Materials Today: Proceedings*, 72, 3890-3895

Merimi C., Hammouti B., Zaidi K., Hafez B., Elmsellem H., Touzani R., Kaya S., (2023). Acetylsalicylic acid as an environmentally friendly corrosion inhibitor for carbon steel XC48 in chloride environment, *Journal of Molecular Structure,* 1278, 134883

Mu G.N., Li X., Li F., (2004) Synergistic inhibition between o-phenanthroline and chloride ion on cold rolled steel corrosion in phosphoric acid, *Mater. Chem. Phys.,* 86, 59–68

Nahl´e A., Salim R., El. Hajjaji F., Aouad M.R., Messali M., Ech-Chihbi E., Hammouti B., Taleb M., (2021) Novel triazole derivatives as ecological corrosion inhibitors for mild steel in 1.0 M HCl: experimental & theoretical approach, *RSC Adv.,* 11, 4147–4162

Noor E.A., Al-Moubaraki A.H., (2008) Thermodynamic study of metal corrosion and inhibitor adsorption processes in mild steel/1-methyl-4[40(-X)-styryl pyridinium iodides/hydrochloric acid systems, *Mater. Chem. Phys.,* 110, 145–154

Oukhrib R., Abdellaoui Y., Berisha A., Abou Oualid H., Halili J., Jusufi K., Ait El Had M., Bourzi H., El Issami S., Asmary F. A., Parmar V. S. , Len C., (2021). DFT, Monte Carlo and molecular dynamics simulations for the prediction of corrosion inhibition efficiency of novel pyrazolylnucleosides on Cu (111) surface in acidic media, *Scientific reports,* 1, 11-18

Paul P.K., Yadav M., (2020) Investigation on corrosion inhibition and adsorption mechanism of triazine-thiourea derivatives at mild steel/HCl solution interface: electrochemical, XPS, DFT and Monte Carlo simulation approach, *J. Electroanal. Chem. J.,* 877, 114599. doi: 10.1016/j.jelechem.2020.114599

Peverati R. and Truhlar D. G., (2012) Performance of the M11 and M11-L density functionals for calculations of electronic excitation energies by adiabatic time-dependent density functional theory, Physical Chemistry Chemical Physics, 14, 11363-11370. doi:10.1039/C2CP41295K

Pradeep-Kumar C. B., Mohana K. N. and Muralidhara H. B., (2015) Electrochemical and thermodynamic studies to evaluate the inhibition effect of synthesized piperidine derivatives on the corrosion of mild steel in acidic medium, *Ionics*, 21, 263–281

Ramezanzadeh M., Bahlakeh G., Sanaei Z., Ramezanzadeh B., (2019) Corrosion inhibition of mild steel in 1 M HCl solution by ethanolic extract of ecofriendlyMangifera indica (mango) leaves: Electrochemical, molecular dynamics, Monte Carlo and ab initio study, *Appl. Surf. Sci.,* 463, 1058– 1077

Saraswata V., Yadav M., Obot I.B., (2020) Investigations on Eco-Friendly Corrosion Inhibitors for Mild Steel in Acid Environment: Electrochemical, DFT and Monte Carlo Simulation Approach, *Colloids and Surfaces*, 599, 124881

Singh A., Ansari K. R., Lin Y., Quraishi M. A., Lgaz H., and Chung I.-M., (2018) Corrosion inhibition performance of imidazolidine derivatives for J55 pipeline steel in acidic oilfield formation water: Electrochemical, surface and theoretical studies, *Journal of the Taiwan Institute of Chemical Engineers,* 1–16

Srivastava V., Haque J., Verma C., Singh P., Lgaz H., Salghi R., (2017) Amino acid based imidazolium zwitterions as novel and green corrosion inhibitors formild steel: Experimental, DFT and MD studies, *Journal of Molecular Liquids,* 244, 340–352

Stern M., Geaby A.L., (1957) Electrochemical Polarization: I. A Theoretical Analysis of the Shape of Polarization Curves, *J. Electrochem. Soc.,* 104, 56

Sudheer A., Quraishi M.A., Ebenso E.E., Natesan M., (2012) Inhibition of Atmospheric Corrosion of Mild Steel by New Green Inhibitors under Vapour Phase Condition, *Int. J. Electrochem. Sci.,* 7(8), 7463-7475

Tan B., Zhang S., Qiang Y., Guo L., Feng L., Liao C., Xu Y., Chen S., (2018). A combined experimental and theoretical study of the inhibition effect of three disulfidebased flavouring agents for copper corrosion in 0.5 M sulfuric acid, *J. Colloid, Interface Sci.,* 526, 268–280

Tao Z., He W., Wang S., Zhang S. and Zhou G., (2012) A study of differential polarization curves and thermodynamic properties for mild steel in acidic solution with nitrophenyltriazole derivative, *Corros. Sci.,* 60, 205–213

Umoren S. A. (2011). Synergistic inhibition effect of polyethylene glycol–polyvinyl pyrrolidone blends for mild steel corrosion in sulphuric acid medium, *J. Appl. Polym. Sci.,* 119, 2072–2084

Umoren S. A., Banera M. J., Alonso-Garcia T., Gervasi C. A. and Mirifico M. V. (2013). Inhibition of mild steel corrosion in HCl solution using chitosan, *Cellulose* 20, 2529–2545

Umoren S.A., Solomon M.M. (2015) Effect of halide ions on the corrosion inhibition efficiency of different organic species–A review, *J. Ind. Eng. Chem.,* 21, 81–100. doi:10.1016/j.jiec.2014.09.033

Wang X., Yang H., Wang F. (2011) An investigation of benzimidazole derivative as corrosion inhibitor for mild steel in different concentration HCl solutions, *Corros. Sci.,* 53, 113–121

Yousefi A., Javadian S., Dalir N., Kakemam J., Akbari J. (2015) Imidazolium-based ionic liquids as modulators of corrosion inhibition of SDS on mild steel in hydrochloric acid solutions: experimental and theoretical studies, *RSC Adv.,* 5, 11697–11713

Yüce A.O., Kardas G., (2012) Adsorption and inhibition effect of 2-thiohydantoin on mild steel corrosion in 0.1M HCl, *Corros. Sci.,* 58, 86–94

Yukna R. A., Callan D. P., Krauser J. T., Evans G. H., Aichelmann-Reidy M. E., Moore K., Cruz R., Scott J.B. (1998) Multi-center clinical evaluation of combination anorganic bovine-derived hydroxyapatite matrix (ABM)/cell binding peptide (P-15) as a bone replacement graft material in human periodontal osseous defects. 6-month results, *Journal of Periodontology,* 69(6), 655-63. doi: 10.1902/jop.1998.69.6.655

Zerfaoui M., Oudda H., Hammouti B., Benkaddour M., Kertit S., Zertoubi M., Azzi M., Taleb M. (2002), Electrochemical studies of the corrosion inhibition of methionine ethyl ester on iron in citric-chloride solution, *Revue de Métallurgie:* (Paris). Vol.99 N° 12, 1105-1110.

Zerfaoui M., Oudda H., Hammouti B., Kertit S., Benkaddour M. (2004). Inhibition of corrosion of iron in citric acid media by aminoacids, Prog. Org. Coat., 51 (2), 134–138. doi:10.1016%2Fj.porgcoat.2004.05.005

Zerga B., Sfaira M., Rais Z., Ebn Touhami M., Taleb M., Hammouti B., Imelouane B., Elbachiri A. (2009) Lavender oil as an ecofrindly inhibitor for mild steel in 1M HCl, *Mater. Tech.,* 97 (5), 297–305

Zhang Z., Tian N., Zhang L., Wu L. (2015) Inhibition of the corrosion of carbon steel in HCl solution by methionine and its derivatives, *Corrosion Science,* 98, 438–449, doi:10.1016/j.corsci.2015.05.048

(2023) ; https://revues.imist.ma/index.php/morjchem/index